Research article

Synthesis of a novel diaquabis(1,10-phenanthroline)copper(II)chloride complex and its voltammetric application for detection of amoxicillin in pharmaceutical and biological samples

Ameha Debalke [a], Adane Kassa [a,b,*], Tihitinna Asmellash [a], Yonas Beyene [a], Meareg Amare [a], Getinet Tamiru Tigineh [a], Atakilt Abebe [a]

[a] Department of Chemistry, College of Science, Bahir Dar University, Ethiopia
[b] Department of Chemistry, College of Natural and Computational Sciences, Debre Markos University, Ethiopia

A B S T R A C T

A one step facile synthesis of the novel diaquabis(1,10-phenanthroline)copper(II)chloride (A$_2$P$_2$CuC) complex is demonstrated. Cyclic voltammetric and electrochemical impedance spectroscopic results revealed potentiodynamic deposition of a conductive electroactive poly(A$_2$P$_2$CuC) film on the glassy carbon electrode surface increasing its effective surface area. In contrast to the unmodified glassy carbon electrode, appearance of an oxidative peak at a reduced potential with over two fold current for amoxicillin at poly(A$_2$P$_2$CuC)/GCE demonstrated its electrocatalytic property attributed to reduce charge transfer resistance and the improved surface area of the electrode surface. Better correlation of the oxidative peak current with square root of scan rate (R^2 = 0.99779) than with scan rate (R^2 = 0.96953) supplemented by slope of 0.58 for log(current) versus log(scan rate) confirmed diffusion controlled irreversible oxidation of amoxicillin. At optimized solution and SWV parameters, current response of poly(A$_2$P$_2$CuC)/GCE showed linear dependence on concentration of amoxicillin (2.0–100.0 μM) with LoD 0.0115 μM. While no amoxicillin was detected in the human blood serum sample, an amount 89.40–100.55% of the nominal level was detected in the analyzed eight tablet brands. Spike recovery in tablet samples (98.90–101.95%) and blood serum sample (102.20–101.37%); interference with an error (%RSD) of 0.00–4.51% in tablet and 0.00–2.10% in serum samples; excellent stability and reproducible results, added with the wide dynamic range and low LoD validated the method for amoxicillin determination in pharmaceutical formulations and human urine samples.

1. Introduction

β-Lactam drugs are the most commonly used antibiotics and have a structure based on a β-lactam ring, which is responsible for the antibacterial activity [1, 2]. Amoxicillin (AMX), is an acid-stable, semi-synthetic drug that belongs to penicillin class of β-lactam antibiotics [3]. AMX, which is one of the vital medications recognized by the World Health Organization (WHO) [4], is a widely used antibiotic in human and veterinary medicine for the treatment and prevention of respiratory, gastrointestinal, urinary, and skin bacterial infections [5, 6]. AMX (Scheme 1) is the only phenolic penicillin and spectrum β-lactam antibiotic [7] and better absorbed following its oral administration being the choice of the β-lactam antibiotics [8], its improper usage may lead to side

effects such as stomach pains, diarrhea, chills, and blood in the urine [9, 10, 11]. As one of the most preferred antibiotics for bacterial infections but associated with side effects on its improper usage, its accurate and precise determination is crucial.

Many analytical techniques for the determination of AMX have been described, including spectrophotometry [12], chromatography [13] and chemiluminescence [14]. However, these techniques are expensive, need complex sample pretreatment, consume large sample volumes, and long analysis time [15, 16]. Advances in electrochemical methods such as cyclic voltammetry, square wave voltammetry, differential pulse voltammetry, and stripping voltammetry with their fast response, high sensitivity, easy operation, and cost-effective [15, 16, 17], have been widely used for the determination of drugs [18, 19]. Recent attempts on
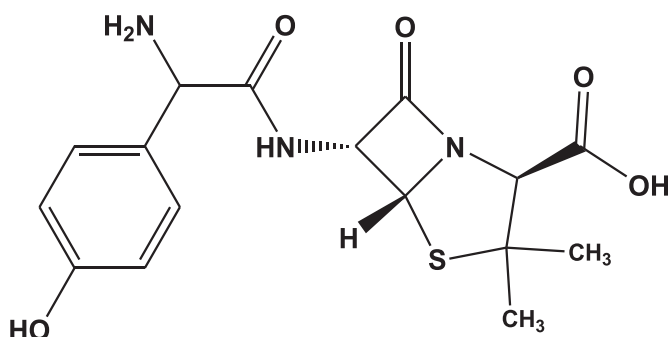
* Corresponding author.
  E-mail address: adanekss97@gmail.com (A. Kassa).

Scheme 1. Structure of amoxicillin.

AMX determination using electrodes modified with various materials include Au-PdNPs/rGO [20], PGA/3D-GE [21], rGO/Nafion [22], Cu/ZnmMOF [23], and poly(AHNSA) [24], most of which have limitations such as high costs, unavailability, and cumbersome modification procedures.

1,10-phenanthroline (phen), which is a bidentate ligand, acts as chelating agent in coordination chemistry [25]. 1,10-phenanthroline and its derivatives interact with metal ions through the nitrogen atom by promoting the synthesis of metal complexes [25, 26]. Showed unique proprieties including high accessible surface area, high chemical stability, and excellent electrocatalytic activity as metal complexes [26, 27]; application of phen based metal complexes for electrochemical sensor fabrication is emerging [26, 27].

This work was aimed at fabrication of a novel poly(diaquabis(1,10-phenanthroline)copper(II)chloride) complex modified glassy carbon electrode for AMX determination in human blood serum and tablet formulation samples, which to the best of our knowledge is not reported for the same.

2. Materials and methods

2.1. Chemicals and apparatus

Amoxicillin trihydrated ($\geq$99.0% Sigma Aldrich), $K_3[Fe(CN)_6]$ and $K_4[Fe(CN)6]$ (98.0% BDH laboratory samples, England), potassium chloride (99.5%, Blulux laboratories (p) Ltd), sodium monohydrogen phosphate and sodium dihydrogen phosphate ($\geq$98.0%, Blulux laboratories (p) Ltd), hydrochloric acid (37%, Fisher Scientific), sodium hydroxide (Extra pure, lab Tech chemicals), nitric acid (70%, Fisher Scientific), $CuCl_2 \cdot 2H_2O$ (99.0%, BDH), 1,10-phenanthroline monohydrate ($\geq$99.7%, Sigma Aldrich), and $AgNO_3$ ($\geq$99.0%, Sigma Aldrich), are among the chemical used. All chemicals were of analytical grade and thus used without further purification.

CHI 760E potentiostat (Austin, Texas, USA), pH meter (AD 8000, Romania), electronic balance (Nimbus, ADAM equipment, USA), refrigerator (Lec refrigration PLC, England), deionizer (Evoqua water technologies), portable pH/conductivity/TDS meter (Bante901P), UV-Vis spectrophotometer (Cary 60, Agilent technologies), FT-IR spectrophotometer (BX, Agilent), ICP-OES spectrometer (PerkinElmer, Optima 7300V HF Version), and melting point apparatus (Stuart SMP30), are among the apparatus/instruments used.

3. Results and discussion

3.1. Synthesized complex

3.1.1. Synthesis mechanism

The $Cu(phen)_2(H_2O)_2]Cl_2$ (A_2P_2CuC) complex was synthesized by one step procedure (Eq. (1)) using phen, and $CuCl_2.2H_2O$ as raw materials (Scheme 2). The results of the studied physicochemical properties of synthesized complex are summarized in Table 1.

$$CuCl_2 \cdot 2H_2O + 2(1, 10 - \text{phenanhroline monohydrate})$$
$$\rightarrow \left[Cu(phen)_2(H_2O)_2\right]Cl_2 \quad (1)$$
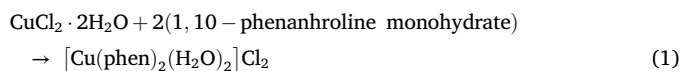
The facile formation of A_2P_2CuC (Scheme 2) may be attributed to the acquisition of thermodynamic stability due to the classic chelating bidentate and strong field ligand properties of phen, supplemented by the formation of octahedral geometry. This is a consequence of the cooperative contributions of its ideally placed nitrogen atoms, its rigid planar structure, and π-acidic properties [28]. The complex being soluble in polar solvents like DMSO and water, its solubility decreases with decreasing polarity of the solvents. The composition was confirmed from gravimetric halide estimation and metal content determination using ICP-OES (Table 1). Furthermore, the high measured conductance of the as-synthesized complex in an aqueous solution (Table 1) might be accounted for the presence of chloride as counter anions.

#### 3.1.2. Characterization of as-synthesized complex

FT-IR, and UV-Vis were used to characterize the synthesized complex. In both cases, changes like disappearance or appearance of peak intensity and distinct peaks were considered as evidences for synthesis of new complex.

3.1.2.1. UV-Vis. The UV-Vis spectra of the Cu(II) salt, phen, and synthesized complex (A_2P_2CuC) in ethanol are presented (Figure 1). From the figure, Cu(II) salt solution exhibited unique absorption bands at about 551 and 569 nm (a) which is characteristic of the d–d transition of free Cu^{2+} [27]. The absorptions due to $\pi \rightarrow \pi^*(C=C)$, $\pi \rightarrow \pi^*(C=N)$ and $n \rightarrow \pi^*(C=N)$ transitions are responsible for the absorption bands at 290, 309, and 323 nm that define the free phen ligand (b), respectively [27, 28]. Compare to the spectrum of the Cu(II) salt (a), shifting of the bands from 551 to 569 nm (a) to 626, and 644 nm, respectively (c) for the complex, confirmed the formation of a new A_2P_2CuC complex [29].

Absence of the bands at 309 and 323 nm, which are characteristic to the transitions $\pi \rightarrow \pi^*$ and $n \rightarrow \pi^*$ of C=N, respectively of 1,10-phenanthroline (Figure 1b), in the spectrum for the as-synthesized complex (Figure 1c) showed the preparation of the complex presumably *via* C=N.

Table 1. Summary of physicochemical properties of A_2P_2CuC complex.

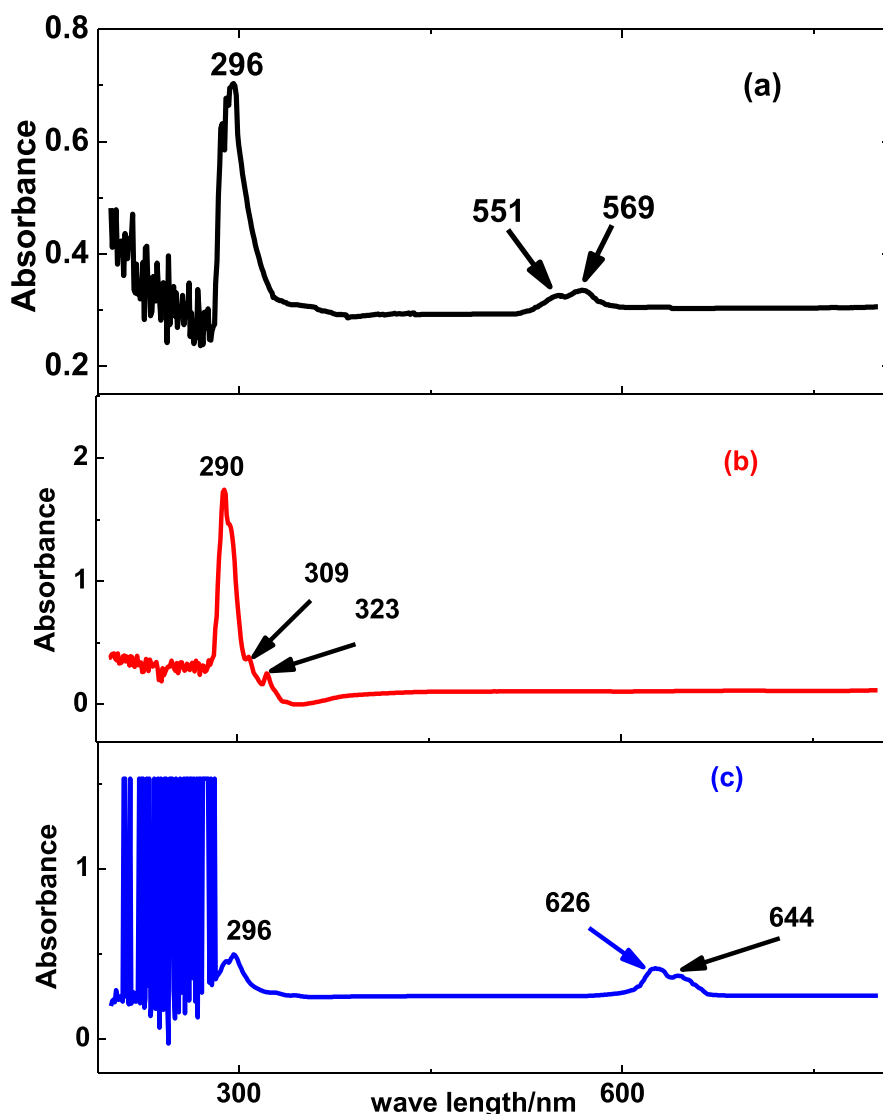| physical property	$[Cu(phen)_2(H_2O)_2]Cl_2$
Color	Spring green
Melting point (°C)	325–327
Solubility	Soluble in H_2O, CH_3CN, DMSO
Stability at room temperature	Stable
Conductivity (S cm^2 mol^{-1})	138
Cu(II): Cl^{-1} mass ratio	12.00:13.36
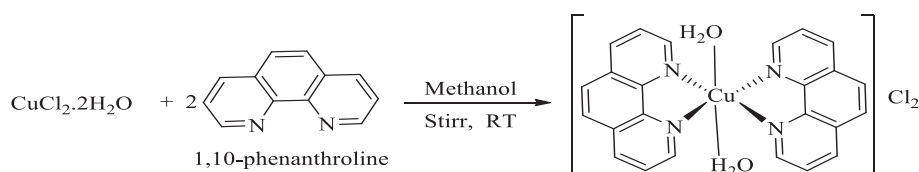
Scheme 2. Synthesis mechanism for A_2P_2CuC.

Figure 1. UV–Vis spectra of $CuCl_2.2H_2O$ (a), phen (b), and A_2P_2CuC (c) in ethanol.

Table 2. Summary of the electronic spectral data of Cu(II) salt, phen, and synthesized complex with proposed transition type.

species	λ_{max} (nm)	type of transition
Cu(II)	296	charge transfer
	551	d-d transition
	569	d-d transition
Phen	290	$\pi \rightarrow \pi^*(C=C)$
	309	$\pi \rightarrow \pi^*(C=N)$
	323	$n \rightarrow \pi^*(C=N)$
A_2P_2CuC	296	charge transfer
	626	$^2B_{1g} \rightarrow \, ^2E_g$
	644	$^2B_{1g} \rightarrow \, ^2B_{2g}$

Moreover, significant decrease of the LMCT band at 296 nm indicated the decrease of number of the σ and π base H_2O as the result of the coordination of two molecules of phen to Cu(II). Table 2 summarized the UV-Vis absorption band wave length results, and proposed transition type for each band of the analyzed species.

3.1.2.2. FT-IR. The FT-IR spectra for the free phen (a), and A_2P_2CuC complex (b) are showed in Figure 2; the vibrational assignments of which

are summarized in Table 3. The overtone band of the free phen at 2067 cm^{-1} (w) (Figure 2a) vanished in the complex, indicating that the compound was coordinated with the metal to create a rigid structure. The band due to νC-N in the free phen (a) at 1352 cm^{-1}(s) was red shifted to 1337 cm^{-1}(w) in the complex (b) verifies that phen was coordinated to the metal ion through its azomethine N atom [28]. A new band was observed at 425 cm^{-1} in the spectrum of the complex (b) which was assigned to νCu-N indicated the coordination of Cu(II) with phen through N. Likewise, the band at 3433 cm^{-1} representing νOH of the water of crystallization of the molecular phen (a) was found shifted to 3397 cm^{-1} in A_2P_2CuC (b) indicating the change in its electronic environment after the formation of the complex albeit it still was a liquid of crystallization. In addition, the blue shift of bands at 3045 cm^{-1} (w), 1624 cm^{-1} (m), 1414 cm^{-1} (s), 1583 cm^{-1} (s) due to νC-H, νC=C, δC=C and νC=N, in the free phen (a) to 3054 cm^{-1} (w), 1631 cm^{-1} (m), 1431 cm^{-1} (s), and 1585 cm^{-1} for A_2P_2CuC (b) observed, respectively is a consequence of increase in electron density in the coordinated phen as a result of the π-back electron donation by Cu(II).

3.2. Preparation of poly(A_2P_2CuC)/GCE

A polymer film of the complex was deposited on the GCE surface from a solution of 1.0 mM A_2P_2CuC complex in pH 7.0 by cycling the potential
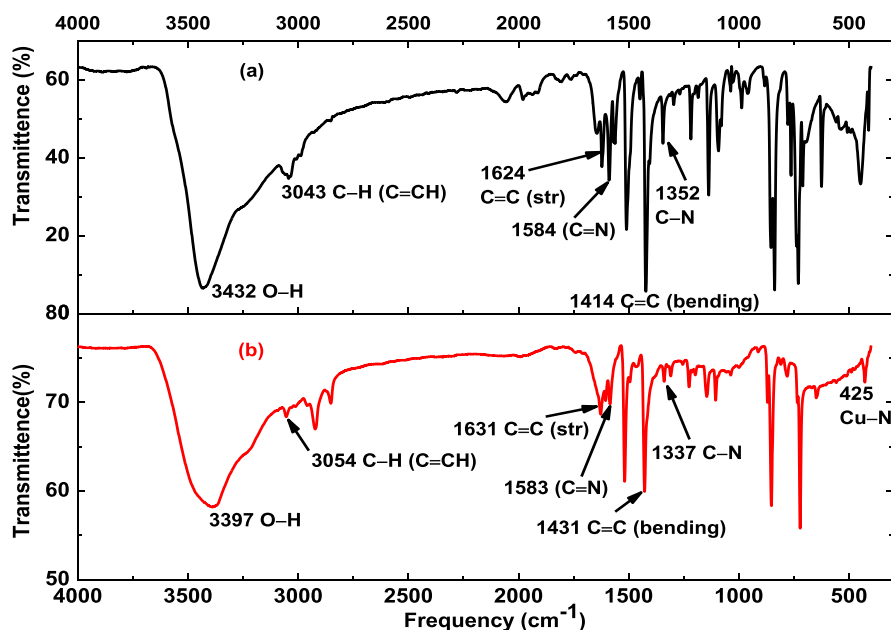
Figure 2. FT-IR spectra of phen (a), and A_2P_2CuC (b).

Table 3. Summary of important characteristic IR bands of the phen and synthesized complex, and proposed vibrational modes.

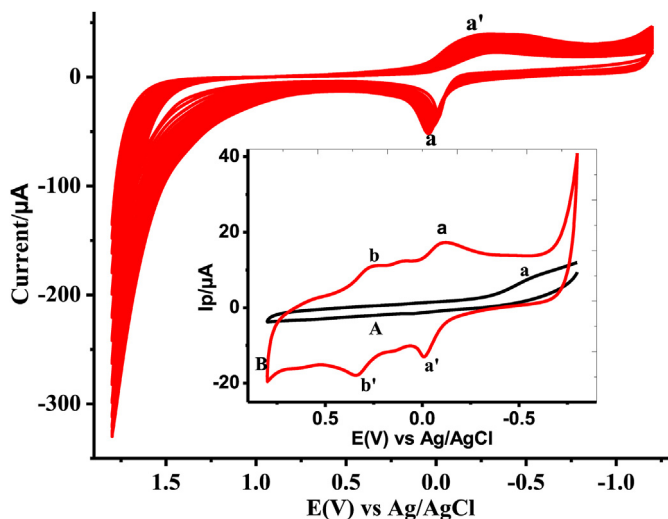| compound	absorption frequencies, cm^{-1}						
	νO-H(H$_2$O)	νC-H	νC=C	δC=C	νC=N	νC-N	Cu-N
Phen	3432(s)	3043(w)	1624(m)	1414(s)	1588(s)	1352(s)	-
A_2P_2CuC	3397(s)	3054(w)	1631(m)	1431(s)	1583(m)	1337(w)	425 (m)

ν = stretching; δ = bending

Figure 3. CVs of GCE in pH 7.0 PBS containing 1.0 mM A_2P_2CuC complex scanned between -1.2 V to +1.8 V at 100 mV s^{-1} for 15 cycles. Inset: CVs of (A) bare GCE and (B) stabilized poly(A_2P_2CuC)/GCE (B) in monomer free 0.5 M H$_2$SO$_4$ at scan rate of 100 mV s^{-1}.

from -1.2 to $+1.8$ V for 15 cycles (Figure 3). During the polymerization process, sharp anodic (peak a) and broad cathodic (peak a′) peaks were observed whose current response increased with increasing scan cycles indicating polymer film growth [30, 31]. Inset of Figure 3 depicts the CVs of unmodified GCE (curve A) and the poly(A_2P_2CuC)/GCE (curve B) in a monomer free 0.5 M of H$_2$SO$_4$ solution. In contrary to the unmodified

electrode which showed a single reductive peak (peak a of inset A) ascribed to reduction of molecular oxygen, appearance of couples of redox peaks (a & a′, and b & b′) at the modified electrode (curve B of inset) confirmed modification of the surface by a redox-active polymer film.

In a A_2P_2CuC complex modified electrode, the anodic peak appeared at $+40$ mV was related to the oxidation process of reduced Cu(0) to Cu(II) in the film, and the corresponding broad cathodic peak centered at about -262 mV was observed due to the reduction process from Cu(II) to Cu(0) [32]. However, the authors still are not able to propose the exact mechanism of the electropolymerization.

3.3. Characterization of poly(A_2P_2CuC)/GCE

The modification of the surface of the GCE by an electroactive complex polymer film of poly(A_2P_2CuC) was additionally verified by results obtained using two techniques; cyclic voltammetry and electrochemical impedance spectroscopy using Fe(CN)$_6^{3-/4-}$ as a probe.

3.3.1. Cyclic voltammetry

Cyclic voltammetry was used to follow the synthesis of a new material based on the features of the resulting voltammograms for both AMX, and Fe(CN)$_6^{3-/4-}$. The repetitive cyclic voltammograms of GCE in a solutions of Cu(II) salt (A), phen (B), and A_2P_2CuC (C) were presents (Figure 4). The voltammogram of each polymerization showed distinct oxidative and reductive peaks with observed potential shift, confirming conversion of salt and the ligand to the complex.

Cyclic voltammograms of bare GCE, Cu(II)/GCE, poly(phen), and poly(A_2P_2CuC)/GCE for the probe are presented in Figure 5 a–d. Appearance of a redox couple at both electrodes is attributed to the
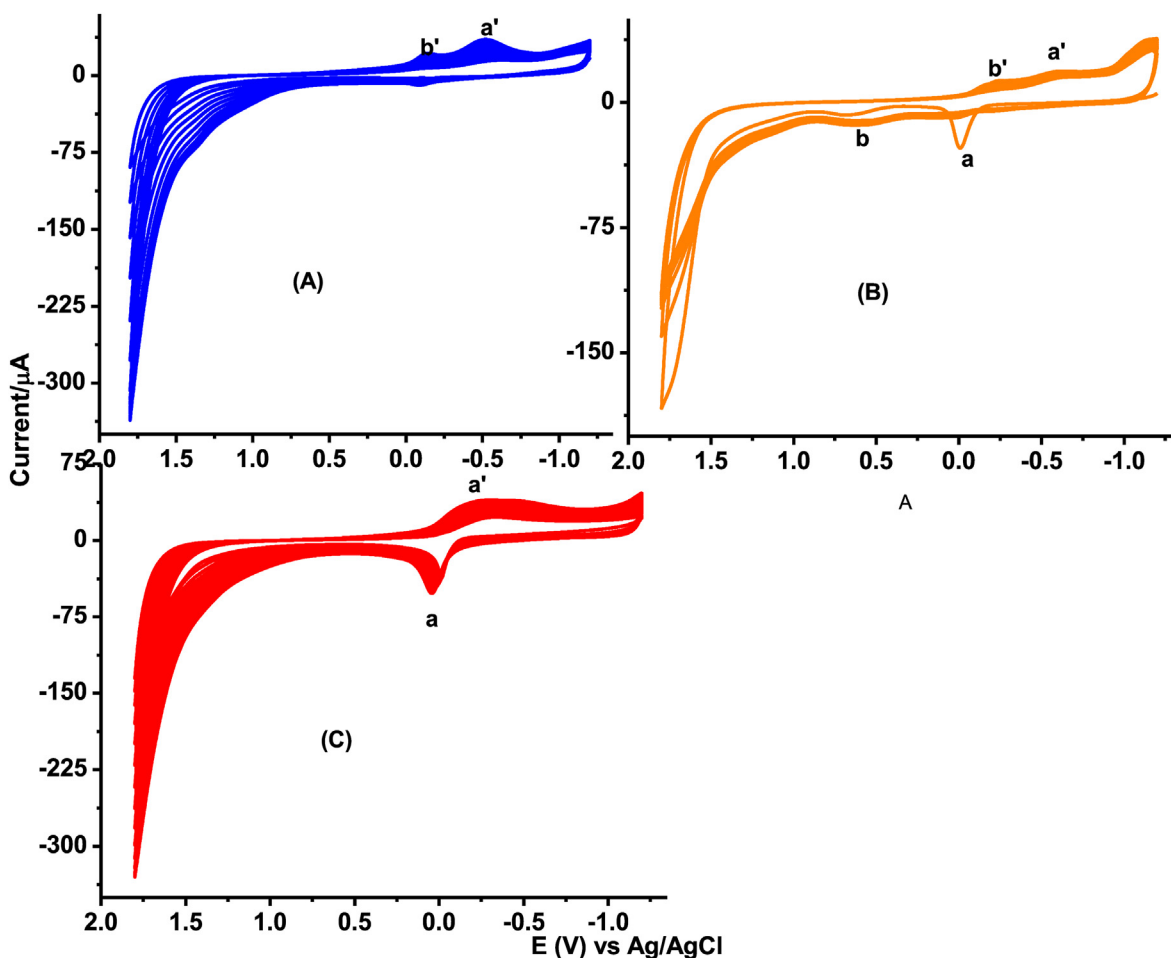
Figure 4. CVs of GCE in pH 7.0 PBS containing 1.0 mM of Cu(II) (A), phen (B), and A_2P_2CuC (C), scanned between -1.2 and $+1.8$ V for 15 cycles at scan rate of 100 mV s^{-1}.

characteristic one electron electrochemical redox process of $[Fe(CN)_6]^{3-/4-}$. The observed peak-to-peak separation (ΔE) reduction from 396 mV at the unmodified GCE (curve a) to 225, 117, and 103 mV at poly(phen)/GCE, Cu(II)/GCE, poly(A_2P_2CuC)/GCE, respectively, and

peak current enhancement at the poly(A_2P_2CuC)/GCE for the probe confirmed the successful deposition of a polymer film on the surface of the GCE [31].

The effective surface area of the electrodes was estimated from the slope value of the plot of Ipa *versus* $\nu^{1/2}$ of the CV response of each electrode for $Fe(CN)_6^{3-/4-}$ using the Randles–Sevcik equation Eq. (2).

$$I_{pa} = 2.69 \times 10^5 n^{3/2} A D^{1/2} \nu^{1/2} C \tag{2}$$

where I_{pa} the anodic peak current, n the number of electron transfer, A the active surface area of the electrode, D the diffusion coefficient, C_o the bulk concentration of $K_3Fe(CN)_6$ and ν is the scan rate.

Effect of scan rate on the current response of the four electrodes for 10.0 mM $K_4Fe(CN)_6$ in pH 7.0 PBS containing 0.1 M KCl electrolyte with n = 1 and D = 7.6×10^{-6} cm s^{-1} were recorded (SM-1 in the supporting material). From the results in Table 4, the calculated effective surface areas of the studied electrodes are in agreement with the observed trend for the current response in SM-1 in the supporting material. Thus, the increased current for the probe at the poly(A_2P_2CuC)/GCE might be
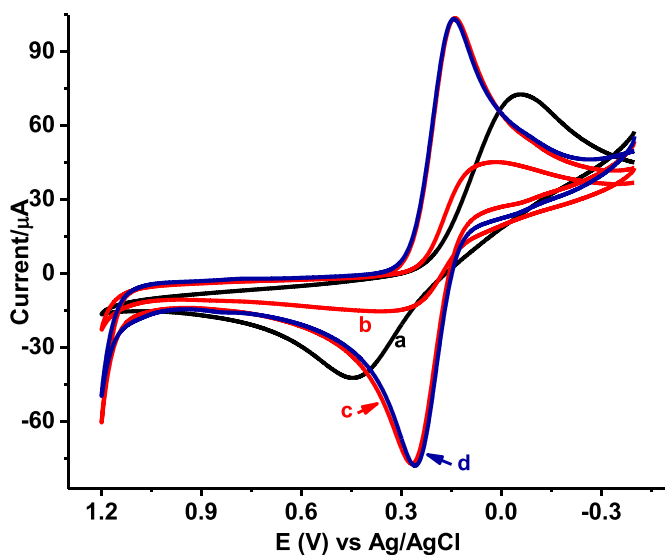
Figure 5. CVs of bare GCE (a), poly(phen)/GCE (b), Cu/GCE (c), and poly(A_2P_2CuC)/GCE (d), in pH 7.0 PBS containing 10.0 mM $[Fe(CN)_6]^{3-/4-}$ and 0.1 M KCl. Scan rate 100 mVs^{-1}.

Table 4. Summary of calculated effective surface area of the electrodes.

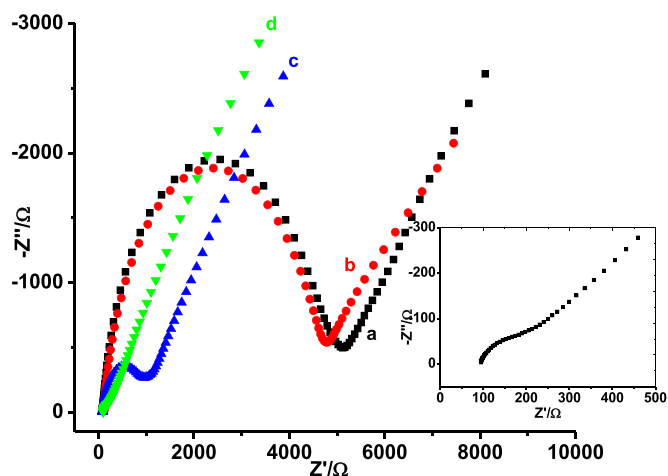| electrode	slope of $(\nu)^{1/2}$ vs Ipa	surface area/cm^2
GCE	4.0	0.054
poly(phen)/GCE	2.1	0.028
Cu/GCE	7.3	0.094
Poly(A_2P_2CuC)/GCE	7.7	0.104

Figure 6. Nyquist plot of (a) bare GCE, (b) poly(phen)/GCE, (c) Cu/GCE, and (d) poly(A_2P_2CuC)/GCE, in pH 7.0 PBS containing 10.0 mM [Fe(CN)^6]$^{3-/4-}$ and 0.1 M KCl in the frequency range: 0.01–100000 Hz, amplitude: 0.01 V, and potential: 0.23 V. Inset: magnified Nyquist plot at high frequency region of the poly(A_2P_2CuC)/GCE.

Table 5. Summary of calculated circuit elements for the studied electrodes.

Electrode	R_s/Ω cm^2	R_{ct}/Ω cm^2	freq/Hz	C_{dl}/F	R_F
GCE	43.9	5362	1412.0	2.1×10^{-8}	1.0
poly(phen)/GCE	43.9	4950	93.3	3.4×10^{-7}	16.2
Cu/GCE	43.9	1452	100.0	1.1×10^{-6}	52.4
Poly(A_2P_2CuC)/GCE	43.9	275	125.9	4.6×10^{-6}	219.0

ascribed to the enhanced active surface area, which is nearly 2.0 times larger than that of the bare GCE.

3.3.2. Characterization by electrochemical impedance spectroscopy

Electrochemical impedance spectroscopy (EIS) measurements by using different electrodes: bare GCE, poly(phen)/GCE, Cu/GCE, and poly(A_2P_2CuC)/GCE were recorded as shown in Figure 6. The Nyquist plots are all composed of semicircles in the high frequency region, and a slopping line in the low frequency region. Comparing the electrodes in terms of selected parameters including the charge transfer resistance (R_{ct}), capacitance (C_{dl}), and roughness factor (R_F) were used to confirm the electrode modification. The Nyquist plots for the unmodified and modified GCE are presented in Figure 6. As can be seen from the figure, all electrodes exhibited a semicircle with varying diameter at the high frequency region and a linear line at low frequency region representing the diffusion of the electroactive species from the bulk to the solution-electrode interface.

Table 5 presents circuit element summary including charge transfer resistance (R_{ct}), solution resistance (Rs), and double layer capacitance (C_{dl}), for each studied electrode as calculated from the respective Nyquist plot using Eq. (3), and roughens of modified electrode (R_F) using Eq. (4).

$$C_{dl} = \frac{1}{2\pi R_{ct}f} \quad (3)$$

where f – frequency corresponding to the maximum imaginary impedance (reactance) value on Nyquist plot.

$$R_F = \frac{C_{dl}}{C_s} \quad (4)$$

where C_{dI} – the double layer capacitance of the modified electrode, and, C_S – capacitance of the smooth surface of the unmodified electrode.
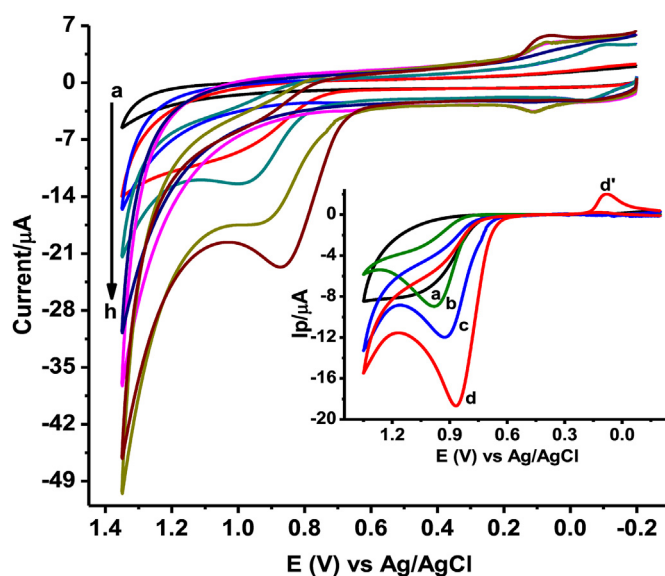

Figure 7. CVs of bare GCE (a & b) poly(phen)/GCE (c & d), Cu/GCE (e & f) and poly(A_2P_2CuC)/GCE (g & h) in the absence (a, c, e & g) and presence (b, d, f & h) of 1.0 mM AMX in pH 7.0 PBS at scan rate 100 mV s^{-1}. Inset: corrected for blank CVs of AMX at (a) bare GCE, (b) poly(phen)/GCE, (c) Cu/GCE, and (d) poly(A_2P_2CuC)/GCE.

The least R_{ct} value (275 Ω) and hence highest C_{dl} (4.6×10^{-6} F) for poly(A_2P_2CuC)/GCE (curve d) demonstrated deposition of a thick poly(A_2P_2CuC) film on the surface of GCE that greatly improves the charge transfer across the solution-electrode interface, may be attributed to the conductive nature of the polymer film. The highest calculated R_F value (ca. 219.0) of the poly(A_2P_2CuC)/GCE also indicated modification of the surface of the electrode by a modifier that increased the roughness of the surface and hence effective surface area responsible to enhance the current response for an analyte.

3.4. Cyclic voltammetric investigation of AMX at poly(A_2P_2CuC)/GCE

3.4.1. Electrochemical behavior of AMX

Since the low R_{ct}, and high R_F values from the EIS analysis of poly(-A_2P_2CuC)/GCE are evidences for an electrode to possess catalytic behavior by reducing over-potential, and enhancing current response of
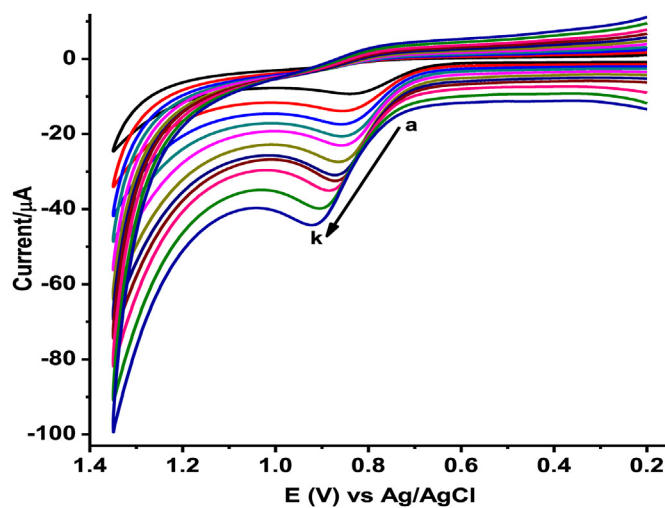

Figure 8. CVs of poly(A_2P_2CuC)/GCE in pH 7.0 PBS containing 1.0 mM AMX at various scan rates (a–k: 20, 40, 60, 80, 100, 125, 150, 175, 200, 250, and 300 mV s^{-1}, respectively).
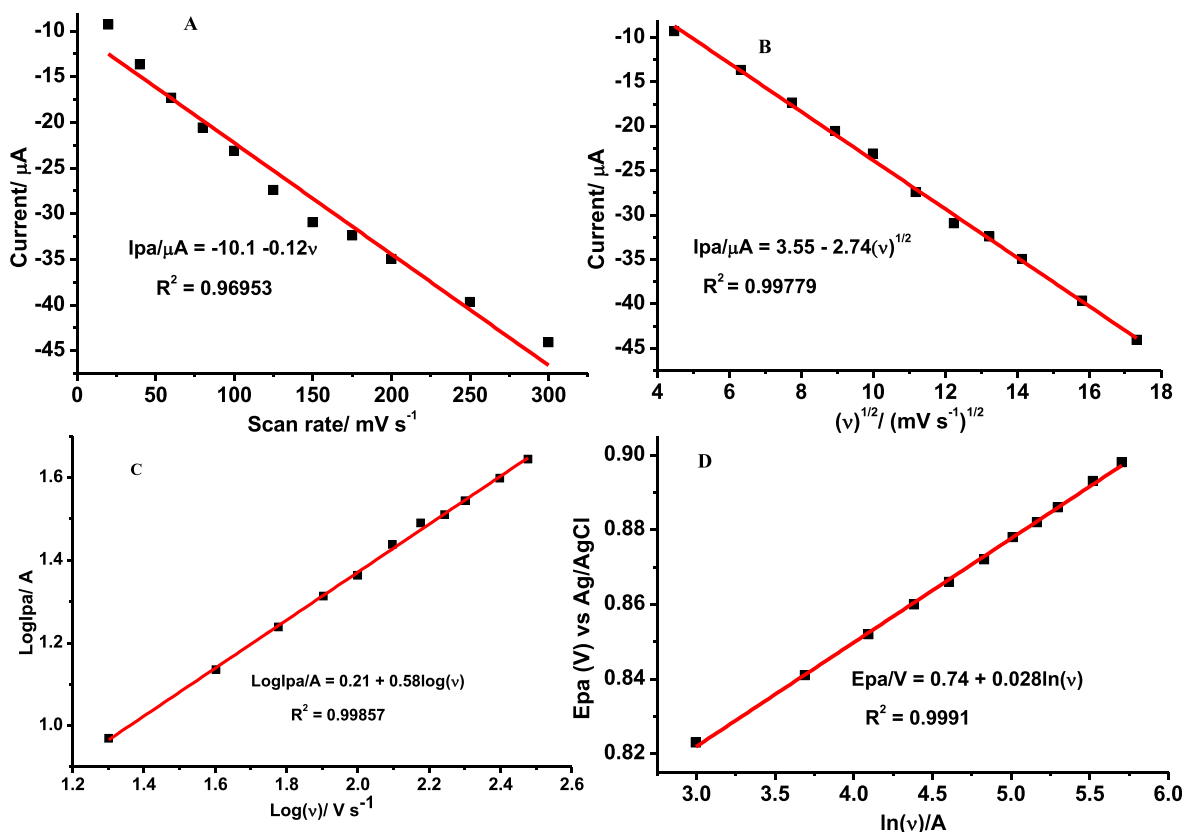
Figure 9. plot of (A) Ip versus scan rate, (B) Ip versus $\nu^{1/2}$, (C) log(Ip) versus log(ν), and (D) Ep versus ln(ν).

an electroactive species, electrochemical behavior of AMX was examined at the poly(A_2P_2CuC)/GCE.

Cyclic voltammograms of AMX at bare GCE, poly(phen), Cu/GCE, and poly(A_2P_2CuC)/GCE are presents (Figure 7). As presented in the inset of Figure 7, while the unmodified, poly (phen), and Cu/GCE electrode showed only oxidative peak for AMX (curve a-c of inset), the polymer modified electrode revealed an oxidative peak with much enhanced current at lower potential (a of curve d), and a new reductive peak (a') for AMX. Meanwhile the observed current enhancement for the oxidative peak of AMX (peak a) at the polymer modified electrode be speculated to the increased electrode surface area and surface roughness factor (R_F), appearance of a new reductive peak (a') in agreement to literature [16, 31] and over-potential reduction of the oxidative peak (a) at the polymer modified electrode could be ascribed to the improved charge transfer resistance (R_{ct}) value.

3.4.2. Effect of scan rate on peak potential and peak current

Intending to extract a supporting evidence for the irreversibility of the oxidation of AMX at the polymer modified electrode, and collect some more kinetic parameters, the effect of scan rate on its peak potential and peak current was investigated. Figure 8 presents voltammograms of poly(A_2P_2CuC)/GCE in AMX solution recorded in the scan rate range of 20–300 mV s^{-1}. The observed peak potential shift of AMX with increasing scan rate (Figure 8) confirmed the irreversibility of the oxidation of AMX.

Lower determination coefficient ($R^2 = 0.96953$) for the dependence of the oxidative peak current on the scan rate (Figure 9A) than on the square root of scan rate ($R^2 = 0.99779$) (Figure 9B) indicated that the oxidation of AMX at the poly(A_2P_2CuC)/GCE was predominantly diffusion mass transport controlled [27]. This was further confirmed by the slope value of 0.58 for the plot of log peak current *versus* log scan rate (Figure 9C), which is in agreement with the value of 0.50 for an ideally diffusion controlled reaction [33].

The number of electrons involved during oxidation of AMX at the poly(A_2P_2CuC)/GCE was estimated from cyclic voltammetric data. For an irreversible process, the value of αn was determined by the difference between the peak potential (E_p) and the half-wave potential ($E_{1/2}$) employing Eq. (5) [34].

$$E_p - E_{1/2} = 48/\alpha n \tag{5}$$

where α is the charge transfer coefficient and n is the number of electrons transferred.

Taking E_p and $E_{p1/2}$ for the cyclic voltammogram at a scan rate of 100 mV s^{-1} (Figure 8) to be 863 and 763 mV, respectively, the value of αn was calculated 0.48. The relationship between E_p and lnν for an irreversible oxidation process obeys Eq. (6) [35].

$$E_p = E^0 + \frac{RT}{(1-\alpha)nF}\left\{0.780 + \ln\left(\frac{D_R^{1/2}}{k^0}\right) + \ln\left[\frac{(1-\alpha)nF\nu}{RT}\right]^{1/2}\right\} \tag{6}$$

where E_P is the peak potential, E^0 is the formal potential, α is the electron transfer coefficient, k^0 (s^{-1}) is the electrochemical rate constant, and the other parameters have their usual meanings.

From the slope value of the plot of E_p *versus* ln(scan rate) (Figure 9D) $\left(slope = \frac{RT}{2(1-\alpha)nF} = 0.028\right)$, the value of n(1-$\alpha$) at the experimental temperature of 25 °C was calculated to be 0.46. Taking 0.48 as value of αn from Eqs. (5) and (0).46 for n(1-α) from Eq. (6); n and α were calculated to be 0.94 ($\approx$1.0), and 0.51, respectively, which represented a one electron irreversible oxidation reaction of AMX at the polymer modified electrode.

3.4.3. Effect of pH on peak potential and peak current

To determine if a proton has participated in the reaction, to determine the proton:electron ratio, and to suggest plausible reaction mechanisms, it is helpful to investigate the influence of pH on the peak current and
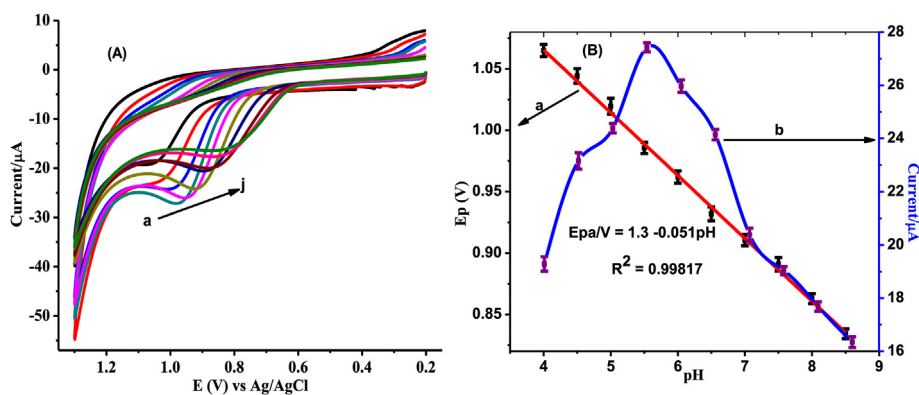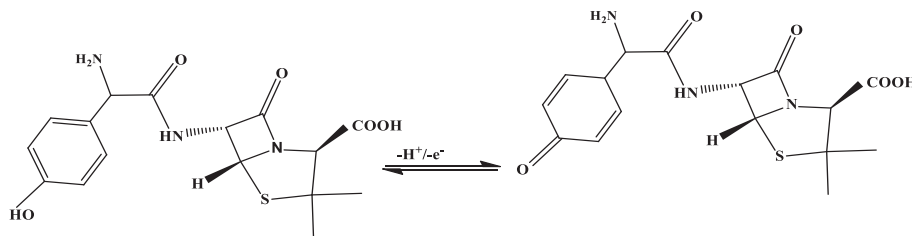
Figure 10. (A) CVs of poly(A$_2$P$_2$CuC)/GCE in PBS of various pHs (a–i: 4.0, 4.5, 5.0, 5.5, 6.0, 6.5, 7.0, 7.5, 8.0, 8.5, respectively) containing 1.0 mM AMX, (B) plot of average peak potential (a) and peak current (b) *versus* pH in the entire studied pH range.

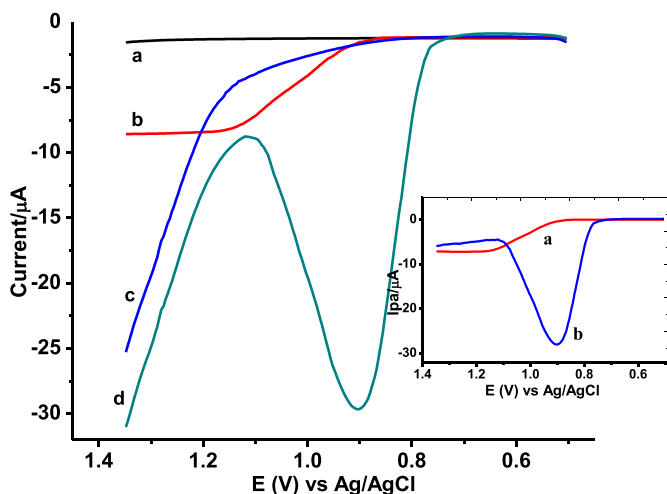**Scheme 3.** Proposed oxidation reaction mechanism of AMX.

Figure 11. SWVs of unmodified GCE (a & b), and poly(A$_2$P$_2$CuC)/GCE (c & d) in pH 5.5 PBS containing no AMX (a & c), 1.0 mM AMX (b & d) at step potential 6 mV, amplitude 35 mV, and frequency 25 Hz. Inset: background corrected SWVs of a) unmodified, and b) poly(A$_2$P$_2$CuC)/GCE.

peak potential of an electroactive species at an electrode. While observed peak potential shift in the negative direction with pH variation from 4.0 to 8.5 (Figure 10A) indicated proton participation during AMX oxidation at the poly(A$_2$P$_2$CuC)/GCE, slope of 0.051 for the plot of oxidative peak potential *versus* pH (curve a of Figure 10B) showed involvement of protons and electrons in a 1:1 ratio [36]. Hence, an irreversible oxidation reaction mechanism involving one electron and one proton was proposed (Scheme 3) for AMX at poly(A$_2$P$_2$CuC)/GCE, which is in agreement with reported mechanism [37, 38, 39]. Moreover, the AMX oxidative peak current at the surface of poly(A$_2$P$_2$CuC)/GCE was observed to increase with pH value from pH 4.0 to 5.5, which then decreased at pH values beyond it (curve b of Figure 10B) making pH 5.5 the optimum as reported elsewhere [24].

3.5. Square wave voltammetric investigation of AMX at poly(A$_2$P$_2$CuC)/GCE

The fact that square wave voltammetry is strong to recognize Faradaic current from non-Faradaic current than cyclic voltammetry [15, 31, 40]. It is used in this work for quantification of AMX in human blood serum samples and various brands of tablet. As a compromise between the current response enhancement with increasing any of the three square wave parameters, and the accompanied capacitive current enhancement causing peak shape distortion, 6 mV, 25 Hz, and 35 mV were taken as the optimum step potential (E_{step}), frequency (f), and amplitude (E_{amp}), respectively (SM-2A-C in the supporting material).
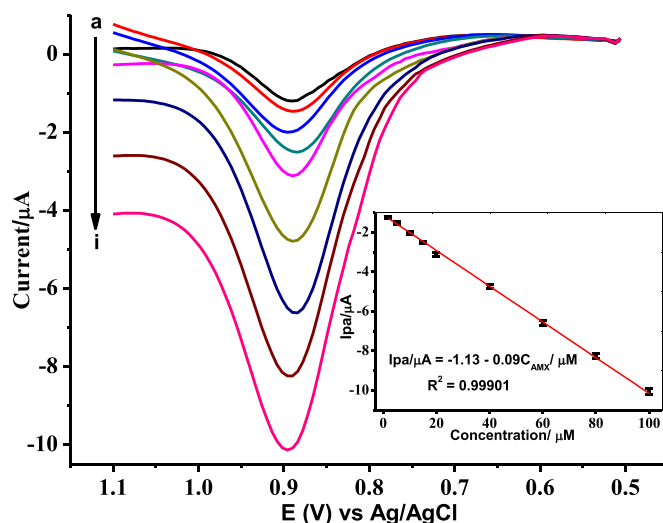

Figure 12. Background corrected SWVs of poly(A$_2$P$_2$CuC)/GCE in pH 5.5 PBS containing various concentrations of AMX (a–i: 2.0, 5.0, 10.0, 15.0, 20.0, 40.0, 60.0, 80.0, and 100.0 μmol L^{-1}, respectively) at E_{step} 6 mV, E_{amp} 35 mV, and f 25 Hz. Inset: plot of average oxidative peak current (mean ± %RSD for n 3) *versus* concentration of AMX.

Table 6. Summary of detected AMX content, and percent detected as compared to the nominal level (20.0 μM) for each of the eight tablet brands, all labeled 500 mg AMX/tablet.

tablet brand	detected AMX in		[c]detected AMX (%)
	[a]sample (μM)	[b]tablet (mg/tablet)	
APF	19.88 ± 0.023	497.00	99.40
CSPC	19.00 ± 0.032	475.00	95.00
Remedica	19.44 ± 0.023	486.00	97.20
EPHARM	18.11 ± 0.025	452.75	90.55
EIPICO	17.88 ± 0.022	447.00	89.40
GSK	20.11 ± 0.020	502.75	100.55
Denk	19.44 ± 0.021	486.00	97.20
Kopran	18.66 ± 0.024	466.50	93.30

[a] detected mean ± %RSD for n = 3;
[b] detected per tablet.
[c] detected relative to company's label.

Figure 11 presents square wave voltammograms of AMX in pH 5.5 PBS at bare GCE (a) and poly(A_2P_2CuC)/GCE (b). Compared to the oxidative peak at 1165 mV with 7.08 μA current at the unmodified electrode (curve a of inset), appearance of a well-shaped oxidative peak at a significantly reduced potential (900 mV) with four folds enhanced current (28.17 μA) at the poly(A_2P_2CuC)/GCE (curve b of inset) signified the catalytic role of the poly(A_2P_2CuC)/GCE towards the oxidation of AMX.

3.5.1. Calibration curve

Figure 12 presents square wave voltammograms of various concentrations of standard AMX in pH 5.5 PBS at poly(A_2P_2CuC)/GCE under the optimized method parameters. In this study, the current response of the polymer modified electrode showed linear dependence on the concentration of AMX in the range of 2.0×10^{-6}–1.0×10^{-4} M (Inset of Figure 12) with a limit of detection (3 s/m, for n = 5) and limit of quantification (10 s/m) of 1.15×10^{-8} M and 3.85×10^{-8} M, respectively. The low associated %RSD values (below 3.5% for n = 3) showed the precision (inset).

3.5.2. Poly(A_2P_2CuC)/GCE for SWV determination of AMX in real samples

3.5.2.1. Determination of AMX in tablet sample.
Square wave voltammograms for the eight tablet brands, each with 20 μM nominal AMX, were recorded (SM-3 in the supporting material). The AMX content detected in each of the eight tablet brands, and compared with the company's label are summarized in Table 6.

As can be seen from the table, the detected AMX content ranged between 89.40 (EIPICO) and 100.55% (GSK) of what was expected with % RSD values below 3.20% (n = 3). In contrast to the expected level of AMX in the eight studied tablet brands, observed slight deviation from the nominal values may be accounted for experimental errors like possible mass loss during preparation, sort of degradation during storage, otherwise company error during preparation.

3.5.2.2. Determination of AMX in human blood serum sample.
The developed method was further applied for determination of AMX in human blood serum samples prepared as described under the experimental section in supporting material. Absence of a peak at about 0.89 V for AMX (curve a of Figure 13) indicated absence of detectable amount of AMX in the serum sample.

3.6. Spike and interference recovery studies

3.6.1. Spike recovery study

To evaluate the accuracy of the developed SWV method based on poly(A_2P_2CuC)/GCE for its applicability to determine AMX in real
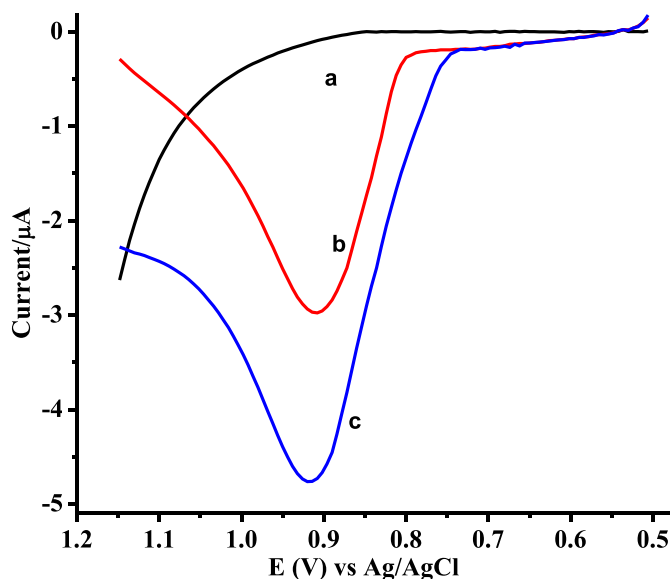

Figure 13. Blank subtracted SWVs of poly(A_2P_2CuC)/GCE in pH 5.5 PBS containing human blood serum samples spiked with various AMX (a–c: 0.0, 20.0, and 40.0 μM, respectively).

Table 7. Summary of spike recovery results of AMX in human blood serum samples.

sample	AMX before spike (μM)	spiked AMX (μM)	detected AMX (μM)[*]	recovery (%)
blood serum	ND	20.0	20.44 ± 0.024	102.20
		40.0	40.55 ± 0.016	101.37

[*] mean±%RSD for n = 3; ND not detected.

samples, recovery studies for spiked AMX in both tablet and human blood serum samples was conducted.

3.6.1.1. Spike recovery from human blood serum sample.
As demonstrated under 3.5.2.2, the blood serum found free of AMX, was spiked with 20.0, and 40.0 μM standard AMX and analyzed for spike recovery.

Figure 13 presents the SWVs for the serum samples before and after spike (a–c: unspiked, 20.0 μM, and 40.0 μM, respectively). As can be seen from the figure, a peak started to appear when the blood serum was spiked with standard AMX, the current of which increased with concentration. Spike recovery results of 102.20% for 20.0 and 101.37% for 40.0 μM spiked AMX with %RSD (n = 3) under 2.4% (Table 7) confirmed the accuracy and hence validity of the method for determination of AMX in human blood serum samples.

3.6.1.2. Spike recovery in tablet samples.
Spike recovery in tablet samples was conducted by taking the tablet brands that showed the least (EIPICO), and the highest (GSK) amount of AMX relative to the nominal value (Figure 14). Tablet samples spiked with 20.0, and 40.0 μM of AMX were checked for the recovery of the respected spiked amounts.

Spike recovery results in the range 98.90% for GSK spiked with 20.0 μM–101.95% for GSK spiked with 40.0 with %RSD (n = 3) under 2.2% (Table 8) confirmed the accuracy of the developed method. From this, it could be concluded that the low AMX content detected in the AMX brands of tablets (Table 6) is not due to low performance of the method but due to lower AMX content than the labels.

3.6.2. Interference study

To further validate the developed method for its applicability for determination of AMX in real samples, its selectivity for AMX in the presence of selected potential interferents was studied.
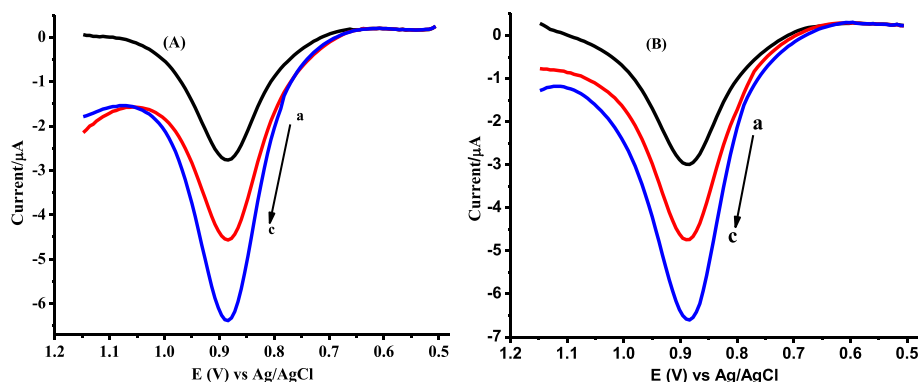
Figure 14. Background corrected SWVs of poly(A$_2$P$_2$CuC)/GCE in pH 5.5 PBS containing (A) EIPICO, and (B) GSK brand tablet samples spiked with different concentrations of AMX (a–c: 0.0, 20.0, and 40.0 μM, respectively).

Table 8. Summary of spike recovery results of AMX from two selected tablet brands (EIPICO, & GSK).

tablet brand	AMX before spike (μM)	spiked AMX (μM)	AMX after spike (μM)[a]	recovery (%)
EIPICO	17.88	-	17.88 ± 0.022	-
		20.00	38.11 ± 0.012	101.15
		40.00	58.22 ± 0.010	100.85
GSK	20.11	-	20.11 ± 0.020	-
		20.00	39.89 ± 0.012	98.90
		40.00	60.89 ± 0.011	101.95

[a] mean±%RSD for n = 3.

Table 9. Summary of interference results of AMX from tablet samples in the presence of various concentrations of AMP, AA, and Glu.

interferent	added (μM)	detected (μA)	expected (μA)	%error
AMP	-	2.88	2.88	-
	10.0	2.81	2.88	0.78
	20.0	2.86	2.88	0.69
	30.0	2.93	2.88	1.73
	40.0	2.99	2.88	3.81
AA	-	2.88	2.88	-
	10.0	2.79	2.88	3.13
	20.0	2.84	2.88	1.39
	30.0	2.94	2.88	2.08
	40.0	2.99	2.88	3.81
Glu	-	2.88	2.88	-
	10.0	2.75	2.88	4.51
	20.0	2.84	2.88	1.39
	30.0	2.94	2.88	2.08
	40.0	2.97	2.88	3.13

Table 10. Summary of interference recovery results of 40.0 μM AMX in human blood serum sample in the presence of different concentrations (20.0–80.0 μM) of Glu, and UA.

interferent	added (μM)	detected (μA)	expected (μA)	%error
Glu	-	4.77	4.77	-
	20.0	4.68	4.77	1.88
	40.0	4.69	4.77	1.68
	60.0	4.77	4.77	-
	80.0	4.87	4.77	2.10
UA	-	4.77	4.77	-
	20.0	4.68	4.77	1.88
	40.0	4.74	4.77	0.63
	60.0	4.84	4.77	1.47
	80.0	4.85	4.77	1.68

spiked AMX in blood serum sample was investigated (SM-5 in the supporting material). Detection of the claimed AMX amount in the serum sample in the presence of the potential interferents at (0, 20.0, 40.0, 60.0, and 80.0 μM) levels with an associated error under 2.10% (Table 10) showed the selectivity of the method for AMX.

3.7. Stability studies

The stability of the modified electrode was evaluated taking five results for 1.0 mM AMX in pH 5.5 with %RSD of 1.14% for five successive SWV measurements recorded at an interval of 2 h in a day (SM-6A in the supporting material) and with an error of (%RSD) 2.4% for five SWV measurements in ten days recorded at an interval of two days (SM-6B in the supporting material), showed the stability of the modifier and hence reproducibility of the results.

In general, excellent spike, and interference recovery results, high precision demonstrated by low %RSD values, and stability of the modified electrode added with the wide linear range and low LoD validated the method for determination of AMX in pharmaceutical and biological samples with complex matrix.

3.8. Performance evaluation of the present method with reported methods

Comparing the performance of the current method to recently reported methods in terms of LoD, linear dynamic range, and modified material allowed for an evaluation of its effectiveness. Our developed method using a novel synthesized complex modified electrode (poly(-A$_2$P$_2$CuC)/GCE) showed the least LoD in addition to a wider linear dynamic range compared to most recent reported methods, which required expensive surface modifiers (Table 11). Hence, the developed method

3.6.2.1. Interference from tablet samples.
The effect of each selected potential interferent (ampicillin (AMP), ascorbic acid (AA), and glucose (Glu)) at its various levels on the response of the method for 20 μM AMX in GSK brand tablet sample was investigated (SM-4 in the supporting material). Detection of the claimed AMX content with an associated maximum error of 4.51% in the presence of the selected potential interferents even at their 200% level (Table 9) showed the selectivity of the method and hence validating its applicability for determination of AMX in tablet samples.

3.6.2.2. Interference from human blood serum sample.
The effect of Glu, and Uric acid (UA) in their various levels on the detection of 40.0 μM

Table 11. Performance of the developed method in contrast to selected reported works.

Substrate	modifier	Dynamic range (μM)	LoD (μM)	refs.
GCE	CB–DHP	2–16.1	0.12	[1]
GCE	AuNP–PdNP-ErGO	30–350	9.0	[20]
GCE	PGA/3D-GE	2–60	0.118	[21]
GCE	rGO/Nafion	1.8–5.4	0.36	[22]
GCE	Cu/Zn-mMOF	1.0–205	0.36	[23]
GCE	Poly(AHNSA)	10–150	0.0099	[24]
GCE	Poly(A_2P_2CuC)	2–100	0.0115	This work

using a novel complex modifier can be an excellent candidate for the determination of AMX in different real samples.

4. Conclusion

While UV-Vis and IR results showed synthesis of the novel complex (A_2P_2CuC), electrochemical impedance spectroscopic and cyclic voltammetric results further verified deposition of a conductive electroactive polymer film of the complex (poly(A_2P_2CuC)) on the surface of glassy carbon electrode, which improved the conductivity, roughness, and effective area of the electrode surface. With remarkable selectivity, sensitivity, stability, and electrocatalytic activity, poly(A_2P_2CuC)/GCE was able to accurately detect amoxicillin in tablet samples from eight different brands. The square wave voltammetric technique created in this study employing poly(A_2P_2CuC)/GCE will serve as a useful guide for the use of analogous conducting polymers in electrochemical sensing.

Declarations

Author contribution statement

Adane Kassa: Conceived and designed the experiments; Performed the experiments; Analyzed and interpreted the data; Contributed reagents, materials, analysis tools or data; wrote the paper.

Ameha Debalke: Conceived and designed the experiments; Performed the experiments; Analyzed and interpreted the data; wrote the paper.

Atakilt Abebe: Performed the experiments; Analyzed and interpreted the data; Contributed reagents, materials, analysis tools or data: wrote the paper.

Meareg Amare: Conceived and designed the experiments; Analyzed and interpreted the data; Contributed reagents, materials, analysis tools or data; Wrote the paper.

Yonas Beyene, Tihitinna Asmellash, Getinet Tamiru Tigineh: Contributed reagents, materials, analysis tools or data; Wrote the paper.

Funding statement

Data availability statement

Data will be made available on request.

Declaration of interests statement

The authors declare no conflict of interest.

Additional information

Supplementary content related to this article has been published online at https://doi.org/10.1016/j.heliyon.2022.e11199.

References

[1] P.B. Deroco, R.C. Rocha-Filho, O. Fatibello-Filho, A new and simple method for the simultaneous determination of amoxicillin and nimesulide using carbon black within a dihexadecylphosphate film as electrochemical sensor, Talanta 179 (2018) 115–123.

[2] S. Yuan, Z. Liu, H. Yin, Z. Dang, P. Wu, N. Zhu, Z. Lin, Trace determination of sulfonamide antibiotics and their acetylated metabolites via SPE-LC-MS/MS in wastewater and insights from their occurrence in a municipal wastewater treatment plant, Sci. Total Environ. 653 (2019) 815–821.

[3] A. Elizalde-Velázquez, L.M. Gómez-Oliván, M. Galar-Martínez, H. Islas-Flores, O. Dublán-García, N. SanJuan-Reyes, Amoxicillin in the aquatic environment, its fate and environmental risk, in: M.L. Larramendy, S. Soloneski (Eds.), Environmental Health Risk-Hazardous Factors to Living Species, IntechOpen, London, 2016, pp. 247–267.

[4] F. Angulo, P. Collignon, J. Powers, T. Chiller, A. Aidara-Kane, F. Aarestrup, World Health Organization ranking of antimicrobials according to their importance in human medicine: a critical step for developing risk management strategies for the use of antimicrobials in food production animals, Clin. Infect. Dis. 49 (1) (2009) 132–141.

[5] F. Ağın, Electrochemical determination of amoxicillin on a poly (acridine orange) modified glassy carbon electrode, Anal. Lett. 49 (9) (2016) 1366–1378.

[6] P.T.H. Yen, N.H. Anh, V.T.T. Ha, L.Q. Hung, P.H. Phong, C.T.T. Hien, Electrochemical properties of amoxicillin on an economical, simple graphite pencil electrode and the ability of the electrode in amoxicillin detection, Vietnam J. Chem. 58 (2) (2020) 201–205.

[7] R. Ojani, J.B. Raoof, S. Zamani, A novel voltammetric sensor for amoxicillin based on nickel-curcumin complex modified carbon paste electrode, Bioelectrochemistry 58 (2012) 44–49.

[8] M.F. Bergamini, M.F. Teixeira, E.R. Dockal, N. Bocchi, E.T. Cavalheiro, Evaluation of different voltammetric techniques in the determination of amoxicillin using a carbon paste electrode modified with [N, N'-ethylenebis (salicylideneaminato)] oxovanadium (IV), J. Electrochem. Soc. 153 (5) (2006) E94.

[9] M.F. Olaniyan, B.T. Olusa, Possible metabolic abnormalities of lipids in rabbits given amoxycillin overdose and raw cucumber (Cucumis Sativus) fruit juice, Matrix Sci. Med. 4 (1) (2020) 15–19.

[10] M.F. Olaniyan, D.B. Adepoju, Assessment of plasma iron, transferrin alanine, and aspartate transaminase in amoxicillin overdose supplemented with raw cucumber juice, J. Health Res. Rev. 6 (1) (2019) 17–21.

[11] O. Rann, M. Sharland, P. Long, I.C. Wong, A.A. Laverty, A. Bottle, C.I. Barker, J. Bielicki, S. Saxena, Did the accuracy of oral amoxicillin dosing of children improve after british national formulary dose revisions in 2014? National cross-sectional survey in England, Brit. Med. J. Open 7 (9) (2017) 1–12.

[12] T. Rojanarata, P. Opanasopit, T. Ngawhirunpat, C. Saehuan, S. Wiyakrutta, V. Meevootisom, A simple, sensitive and green bienzymatic UV-spectrophotometric assay of amoxicillin formulations, Enzym. Microb. Technol. 46 (3-4) (2010) 292–296.

[13] K. Xie, L. Jia, D. Xu, H. Guo, X. Xie, Y. Huang, X. Chen, W. Bao, G. Dai, J. Wang, Simultaneous determination of amoxicillin and ampicillin in eggs by reversed-phase high-performance liquid chromatography with fluorescence detection using pre-column derivatization, J. Chromatogr. Sci. 50 (7) (2012) 620–624.

[14] M. Iranifam, K.M. Khabbaz, Cupric oxide nanoparticles-enhanced chemiluminescence method for measurement of β-lactam antibiotics, Luminescence 30 (5) (2015) 625–630.

[15] A. Kassa, M. Amare, A. Benor, G.T. Tigineh, Y. Beyene, M. Tefera, A. Abebe, Potentiodynamic poly(resorcinol)-modified glassy carbon electrode as a voltammetric sensor for determining cephalexin and cefadroxil simultaneously in pharmaceutical formulation and biological fluid samples, ACS Omega 7 (38) (2022) 34599–34607.

[16] M. Hasanzadeh, N. Shadjou, G.M. de la, Current advancement in electrochemical analysis of neurotransmitters in biological fluids, Trends Anal. Chem. 86 (2017) 107–121.

[17] M. Nemakal, S. Aralekallu, L. Mohammed, M. Pari, K. Reddy, L. Sannegowda, Nanomolar detection of 4-aminophenol using amperometric sensor based on a novel phthalocyanine, Electrochim. Acta 318 (2019) 342–353.

[18] R. Islam, H. Luu, S. Kuss, Electrochemical approaches and advances towards the detection of drug resistance, J. Electrochem. Soc. 167 (4) (2020) 1–14.

[19] H. Lima, J. de Silva, E. de Oliveira Farias, P. Teixeira, C. Eiras, L. Nunes, Electrochemical sensors and biosensors for the analysis of antineoplastic drugs, Biosens. Bioelectron. 108 (2018) 27–37.

[20] N. Kumar, R. Goyal, Gold-palladium nanoparticles aided electrochemically reduced graphene oxide sensor for the simultaneous estimation of lomefloxacin and amoxicillin, Sensor. Actuator. B Chem. 243 (2017) 658–668.

[21] C. Chen, X. Lv, W. Lei, Y. Wu, S. Feng, Y. Ding, J. Lv, Q. Hao, S. Chen, Amoxicillin on polyglutamic acid composite three-dimensional graphene modified electrode: reaction mechanism of amoxicillin insights by computational simulations, Anal. Chim. Acta 1073 (2019) 22–29.

[22] M. Valenga, M. Felsner, C. de Matos, E. de Castro, A. Galli, Development and validation of voltammetric method for determination of amoxicillin in river water, Anal. Chim. Acta 1138 (2020) 79–88.

[23] B. Habibi, A. Pashazadeh, L. Saghatforoush, Zn-mesoporous metal-organic framework incorporated with copper ions modified glassy carbon electrode: electrocatalytic oxidation and determination of amoxicillin, Microchem. J. 164 (2021), 106011.

[24] A. Kassa, M. Amare, Poly (4-amino-3-hydroxynaphthalene-1-sulfonic acid) modified glassy carbon electrode for square wave voltammetric determination of amoxicillin in four tablet brands, BMC Chem. 15 (1) (2021) 1–11.

[25] A. Bencini, V. Lippolis, 1, 10-Phenanthroline: a versatile building block for the construction of ligands for various purposes, Coord. Chem. Rev. 254 (17-18) (2010) 2096–2180.

[26] Y. Oztekin, Z. Yazicigil, A. Solak, Z. Ustundag, Z. Kilic, S. Bilge, Surface modification and characterization of phenanthroline nanofilms on carbon substrate, Surf. Interface Anal. 43 (5) (2011) 923–930.

[27] A. Kassa, A. Abebe, M. Amare, Synthesis, characterization, and electropolymerization of a novel Cu (II) complex based on 1, 10-phenanthroline for electrochemical determination of amoxicillin in pharmaceutical tablet formulations, Electrochim. Acta 384 (2021), 138402.

[28] A. Abebe, T. Hailemariam, Synthesis and assessment of antibacterial activities of ruthenium (III) mixed ligand complexes containing 1, 10-phenanthroline and guanide, Bioinorgan. Chem. Appl. 2016 (2016) 1–9.

[29] G. Miessler, D. Yarr, Inorganic Chemistry, third ed., Pearson Education International, Prentice Hall, 2004. https://hostnezt.com/cssfiles/chemistry/Inorganic%20Chemistry%20By%20GARY%20L.%20MIESSLER.pdf.

[30] M. Amare, S. Admassie, Polymer modified glassy carbon electrode for the electrochemical determination of caffeine in coffee, Talanta 94 (2012) 122–128.

[31] A. Bolzán, Electrodeposition of copper on glassy carbon electrodes in the presence of picolinic acid, Electrochim. Acta 113 (2013) 706–718.

[32] A. Kassa, A. Abebe, G. Tamiru, M. Amare, Synthesis of a novel [diresorcinate-1,10-phenanthrolinecobalt (II)] complex, and potentiodynamic fabrication of poly (DHRPCo)/GCE for selective square wave voltammetric determination of procaine penicillin G in pharmaceutical and biological fluid samples, ChemistrySelect 7 (1) (2022), e202103458.

[33] Y. Zhang, S. Yang, X. Chang, H. Guo, Y. Li, M. Wang, W. Li, L. Jiao, Y. Wang, Electrochemical performance and reaction kinetics of an expanded linear ligand based MOF as a novel anode material for sodium-ion batteries, Chem. Commun. 54 (83) (2018) 11793–11796.

[34] E. Mirmomtaz, A.A. Ensafi, H. Karimi-Maleh, Electrocatalytic determination of 6-tioguanine at a p-aminophenol modified carbon paste electrode, Electroanalysis 20 (18) (2008) 1973–1979.

[35] Y.-H. Zhu, Z.-L. Zhang, D.-W. Pang, Electrochemical oxidation of theophylline at multi-wall carbon nanotube modified glassy carbon electrodes, J. Electroanal. Chem. 581 (2) (2005) 303–309.

[36] T. Shang, P. Wang, X. Liu, X. Jiang, Z. Hu, X. Lu, Facile synthesis of porous single-walled carbon nanotube for sensitive detection of 8-hydroxy-2'-deoxyguanosine, J. Electroanal. Chem. 808 (2018) 28–34.

[37] A. Pollap, P. Knihnicki, P. Kustrowski, J. Kozak, M. Gołda-Cępa, A. Kotarba, J. Kochana, Sensitive voltammetric amoxicillin sensor based on TiO₂ sol modified by CMK-3-type mesoporous carbon and gold ganoparticles, Electroanalysis 30 (10) (2018) 2386–2396.

[38] T.M. Prado, F.H. Cincotto, F.C. Moraes, S.A. Machado, Electrochemical sensor-based ruthenium nanoparticles on reduced graphene oxide for the simultaneous determination of ethinylestradiol and amoxicillin, Electroanalysis 29 (5) (2017) 1278–1285.

[39] A. Kassa, M. Amare, Highly selective and sensitive differential pulse voltammetric method based on poly (Alizarin)/GCE for determination of cefadroxil in tablet and human urine samples, Arab. J. Chem. 14 (8) (2021) 103296.

[40] A.M. Santos, A. Wong, F.H. Cincotto, F.C. Moraes, O. Fatibello-Filho, Square-wave adsorptive anodic stripping voltammetric determination of norfloxacin using a glassy carbon electrode modified with carbon black and CdTe quantum dots in a chitosan film, Microchim. Acta 186 (3) (2019) 1–10.